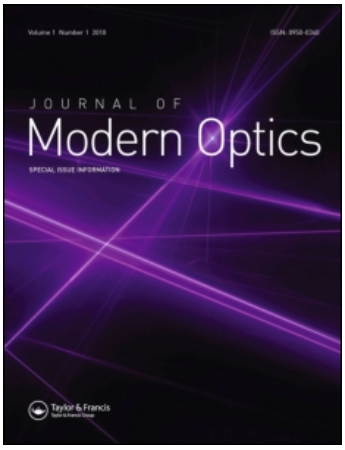

Journal of Modern Optics
Publication details, including instructions for authors and subscription information:
http://www.informaworld.com/smpp/title~content=t713191304

Single-photon counting at 950-1300 nm: using InGaAsP photocathode-GaAs avalanche diode hybrid photomultiplier tubes

Xiaoli Sun[a]; Michael A. Krainak[a]; William E. Hasselbrack[b]; Ross A. La Rue[c]; Derek F. Sykora[c]
[a] NASA Goddard Space Flight Center, Greenbelt, MD, USA [b] Sigma Space Corp., Lanham, MD, USA [c] Intevac, Inc., Santa Clara, CA, USA

To cite this Article Sun, Xiaoli , Krainak, Michael A. , Hasselbrack, William E. , La Rue, Ross A. and Sykora, Derek F.(2009) 'Single-photon counting at 950-1300 nm: using InGaAsP photocathode-GaAs avalanche diode hybrid photomultiplier tubes', Journal of Modern Optics, 56: 2, 284 — 295
To link to this Article: DOI: 10.1080/09500340802364352
URL: http://dx.doi.org/10.1080/09500340802364352

Journal of Modern Optics
Vol. 56, Nos. 2–3, 20 January–10 February 2009, 284–295

Taylor & Francis
Taylor & Francis Group

Single-photon counting at 950–1300 nm: using InGaAsP photocathode–GaAs avalanche diode hybrid photomultiplier tubes

Xiaoli Sun[a]*, Michael A. Krainak[a], William E. Hasselbrack[b], Ross A. La Rue[c] and Derek F. Sykora[c]

[a]*NASA Goddard Space Flight Center, Greenbelt, MD, USA;* [b]*Sigma Space Corp., Lanham, MD, USA;* [c]*Intevac, Inc., Santa Clara, CA, USA*

(*Received 31 January 2008; final version received 24 June 2008*)

We describe the single-photon counting performance of a hybrid photomultiplier tube (HPMT) near-infrared (950–1300 nm) detector with a transfered electron InGaAsP photocathode and a GaAs Schottky avalanche diode anode. These devices have a lower photoelectron multiplication gain than conventional photomultiplier tubes, but offer a greater linear dynamic range and electrical bandwidth. With the use of a low-noise preamplifier, they can detect single photons with a greater than 20% quantum efficiency (QE) and a reasonably low dark-noise count rate. The avalanche diode at the anode operates in a low gain analog mode and has no afterpulsing. As a result, these HPMTs can detect single photons continuously at high count rates without gating. The relatively large photocathode active area (1 mm diameter) is also attractive to many applications including laser altimetry, ranging, and free-space communications through the atmosphere. We measured 25% photocathode QE and nearly the same single-photon detection efficiency at 1064 nm wavelength with a dark count rate of 60,000 per second at −22°C. The output pulse width in response to single-photon detection is about 0.8 ns. The maximum count rate exceeded 100 million counts per second and was limited only by the speed of the electronics. The rms timing jitter of the HPMT output was measured to be about 0.5 ns. The jitter is dominated by the electron diffusion time within the photocathode and can be improved by reducing the photocathode thickness at a small loss in photocathode QE. We evaluated several of these HPMTs and detailed measurement results are reported in this paper.

Keywords: photon counting; PMT; APD

1. Introduction

Single-photon counting detectors are necessary to achieve the highest receiver sensitivity in low light level detection and measurement systems. Many kinds of photon-counting receivers are available at the visible wavelengths, but only a few at near-infrared wavelengths. There is much interest in photon-counting detectors in the 900 to 1600 nm wavelength range because of the availability of diode lasers from the telecommunications industry, the maturity of the technology of Nd:YAG lasers, and recent developments in fiber lasers. At present, the performance of the near-infrared photon-counting detectors is still poor compared to those for visible wavelengths. Commercially available transfered electron (TE) InGaAs photocathode photomultiplier tubes (PMT) typically have a quantum efficiency (QE) of 2% from the 900 to 1600 nm wavelength and a dark count rate under 200,000 per second when cooled to −60°C [1]. Some hand-selected devices can have a QE as high as 10% over this wavelength range, but they often have a higher dark count rate. Similar devices with an InGaAsP photocathode that operate in the 950 to 1300 nm wavelength range have a similar QE but also have a dark count rate as low as 1000 per second [2]. InGaAsP and InP/InGaAs single-photon avalanche photodiodes (SPAD) have a relatively high QE but also a high dark count rate and afterpulsing probability [3–6]. One can cool a SPAD to reduce the dark count rate to an acceptable level, but the afterpulsing probability and the delay time also increase significantly. As a result, most InGaAsP and InP/InGaAs SPADs are used in gated mode with a gating interval of a few nanoseconds and a gate rate of a few kilohertz. Most SPADs can only be used when the arrival times of the photons to be detected are known to within the gate interval, such as in satellite laser ranging or other known target detection, quantum cryptography, and nuclear physics experiments. Another type of near-infrared photon-counting detectors are the InGaAsP TE photocathode hybrid PMTs (HPMTs) that use a GaAs avalanche diode in the gain stage [7–10]. The TE photocathode HPMTs developed by Intevac have demonstrated a QE and a dark count rate similar

*Corresponding author. Email: xiaoli.sun-1@nasa.gov

ISSN 0950–0340 print/ISSN 1362–3044 online

DOI: 10.1080/09500340802364352
http://www.informaworld.com

to those from the best reported InGaAsP and InP/InGaAs SPADs.

The use of an electron bombarded photodiode as the photoelectron multiplication stage inside a PMT was first reported by Kalibjian in 1965 [11]. It was found that photoelectrons from the photocathode can be multiplied upon impact in the space charge region of a reversely biased photodiode. The multiplication gain depends on the energy of the primary photoelectrons at impact, which can be as high as 1000 with a 5 keV electron energy. The resultant hybrid photomultiplier tube consists of only two elements, a photocathode and a semiconductor diode as the anode. The first measurement result of such a hybrid device was reported by DeSalvo et al. in 1992 [12]. The device achieved a gain of several thousand, which was high enough to outperform most avalanche photodiode (APDs) operating in analog mode but still too low for single-photon detection [13]. Cushman and Rusack [14] later developed a hybrid PMT using a large-area APD as the anode to provide additional gain. The total photoelectron multiplication gain reached 10,000, which, in combination with a low-noise preamplifier, is sufficient for single-photon counting applications. The devices are also known as vacuum APDs, electron bombarded APDs, intensified photodiodes (IPDs), hybrid photodiodes, etc. The greatest advantages of HPMTs are the wide dynamic range and low afterpulsing rate, because the photocathode and the APD are operated in linear mode with the bias voltage well below the break-down point. It is also possible to estimate the number of photons within a pulse from the amplitude of the HPMT output. Because there is no dynode chain, the photoelectrons inside an HPMT have a well confined trajectory, and consequently a much lower transit time spread. HPMTs usually have a relatively large active area compared to SPADs, which is a major advantage in receiver optics design and optical alignment. HPMTs are inherently more rugged than conventional PMTs because there are no dynode plates in between the photocathode and anode. Multi-pixel HPMTs can also be constructed by incorporating a multi-element avalanche diode at the anode [7].

HPMTs for visible wavelengths have been available on the market from several manufacturers and they have been used in many applications [15]. Much progress has been made in recent years in InGaAsP and InGaAs photocathode HPMTs for the 950 to 1600 nm wavelength range. The photon-counting detection efficiency (PDE) is now 20–35% over this wavelength range and is comparable to the best InGaAsP SPADs [7,16]. The dark count rate has been reduced to under 60,000 per second at −22°C with a multi-stage thermal electrical cooled (TEC) PMT housing. The afterpulsing rate is negligible and independent of the device temperature. These devices have become very attractive for use in photon-counting laser ranging, atmospheric lidar, and free space optical communications at 950 to 1600 nm wavelengths. They can now be purchased as custom-developed devices.

2. Description of TE photocathode HPMT

A schematic diagram of a TE photocathode HPMT is shown in Figure 1. It consists of a photocathode, an electron bombarded avalanche diode anode, and a set of electron optic focusing baffles. The device is 30 mm in length and 30 mm in diameter and usually potted to protect the high-voltage terminals. The red traces shown in the figure are the electron trajectories which emanate from the 1.0 mm diameter photocathode and which impact on the anode. The design is optimized to provide as tight a focus spot size as possible based on the initial conditions at the cathode with a 45° angular spread in azimuth and elevation and a 0.5 eV starting electron energy. The small spot size intercepting the anode is crucial for reducing anode capacitance and optimizing the bandwidth of the HPMT. The actual spot size is approximately 300 μm in diameter and an oversized 500 μm diameter avalanche diode is used to ease mechanical alignment. At the base of and around the avalanche diode is a half cylinder of metal approximately 3 mm in diameter and 2 mm in length connected to the anode ground plane. When the HPMT is biased, a lateral electric field is produced. The lateral electric field deflects sideways positive ions generated at the anode by the impinging electrons.

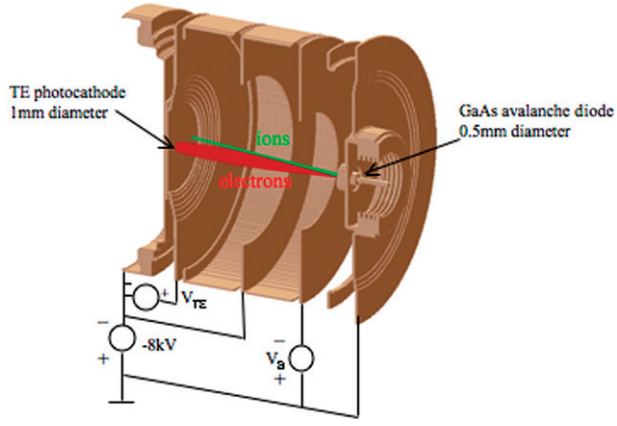

Figure 1. Cross-section of an HPMT and the applied biases (adapted from a SIMION 7.0 electron optics simulation). Photoelectrons (red) from the photocathode are accelerated and focused onto the GaAs avalanche diode anode where a two-stage gain process occurs. Positive ions (green) from the impact are deflected off-axis by the ion deflector electrode at the base of the anode to protect the photocathode and to reduce afterpulsing.

The resulting ion trajectories, shown in green in Figure 1, avoid the photo-active area of the photocathode. This not only protects the photocathode from positive ion bombardment but also minimizes afterpulsing.

The photocathode voltage is typically at −8 kV. A small positive bias voltage (2–4 V) is applied across the TE photocathode. The avalanche diode at the anode is reversely biased at 0.90 to 0.95 times the breakdown voltage. The breakdown voltage varies from device to device and ranges from 35 to 70 V for this type of avalanche diode. Figure 2 shows a photograph of a single-element HPMT from Intevac and the TEC housing made by Products For Research (PFR), Inc.

Timing jitter of the HPMT output can be analyzed as follows. An incident photon, once absorbed to create a photoelectron, undergoes a sequence of events that includes diffusion and drift to the photocathode surface, acceleration in vacuum to the anode, multiplication from the bombardment, and multiplication and diffusion inside the avalanche diode at the anode. The subsequent electronic circuit and threshold detection also introduce jitter. Electron optics analysis using SIMION 7.0 shows that the timing uncertainty for an electron traveling from the photocathode to the anode is less than 13 ps, which is determined by the cathode to anode distance (approximately 2 cm) and the sizes of the photocathode and anode active areas (1.0 mm and 0.5 mm diameters, respectively). The average electron transit time is approximately 3 ns. Timing jitter due to the electron bombardment gain at the anode is also very small because high-energy electrons deposit their kinetic energy in a fraction of a picosecond and within a 1 μm thickness layer of the avalanche diode. The GaAs avalanche diodes used in these devices also have a fast response time with an electrical bandwidth well beyond 1 GHz. The dominant source of HPMT timing jitter is the random walk of the minority carrier electrons across the InGaAsP absorber layer inside the TE photocathode. This can be calculated by solving the time-dependent diffusion equation using a Green's function with appropriate image sources to satisfy the boundary conditions at the front and back of the InGaAsP absorber layer. The resulting expression is algebraically intensive, but an empirical fit to the calculated results can be expressed as

$$\sigma_j \approx \sigma_{\text{diff}} \approx \frac{W^2}{2.62 D_n}, \tag{1}$$

where W is the InGaAsP absorber thickness and D_n is the electron diffusion coefficient. For a 2.5 μm lattice matched InGaAsP absorber layer with a mobility of $3000\,\text{cm}^2\,\text{V}^{-1}\,\text{s}^{-1}$, the photocathode timing jitter is 307 ps, which compares favorably to measured data. One way to reduce the timing jitter is to reduce the InGaAsP absorber layer thickness at the cost of a small loss in quantum efficiency at longer wavelengths. For example, one can reduce the absorber thickness to 1.25 μm to achieve a timing jitter of 77 ps with approximately a one-fifth reduction in quantum efficiency (i.e. from 25% to 20%).

As mentioned earlier, both the InGaAsP TE photocathode and the GaAs avalanche diode within a HPMT are biased below the breakdown voltage and they are not subject to the type of afterpulsing caused by trapped charges filled during the avalanche breakdown, which is the major source of afterpulsing in SPADs. Two potential sources of afterpulsing in an HPMT are positive ion feedback and X-ray feedback to the photocathode. Energetic electrons that intercept the anode can either generate a positive ion at the surface of the anode or an X-ray in the volume of the anode. The positive ion or X-ray can then intercept the cathode creating a pulse of electron charge that is subsequently detected by the anode as an afterpulse. These afterpulses always occur 3 ns or 6 ns after the signal pulse due to the ion and electron transit time between the photocathode and the anode. This has been verified using a Tektronix optical impulse generator (OIG) and a fast oscilloscope. The effect of positive ion feedback has been minimized by the anode electrical field design that deflects the ions away from the active area of the photocathode. The rate of the X-ray generation by the electron bombardment was determined using a special HPMT with an 8 mm diameter GaAs negative electron affinity (NEA) photocathode and a known incident photon rate. The afterpulsing rate was measured to be 2.62×10^{-5} events per incident photoelectron. Since X-rays are emitted from the GaAs anode in random directions,

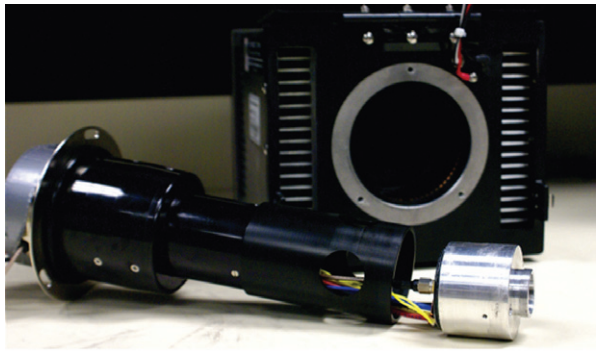

Figure 2. Photograph of a potted HPMT and the TEC housing. An aluminum outer shell was added for ease of alignment. The housing was originally designed for a full-sized PMT and an adapter had to be used to hold the HPMT at the focal point. (The color version of this figure is included in the online version of the journal.)

the afterpulsing efficiency for the HPMT with a 1 mm diameter TE photocathode can be scaled from the above results by the ratio of the solid angles, or 4.1×10^{-7} events per detected photon.

The reliability of the HPMT with InGaAsP photocathodes is under study. Intevac has conducted an initial life test on similar devices. The shelf lifetime was first monitored and devices stored at 20°C for more than 5000 hours have not shown any QE degradation. HPMTs used in the visible wavelength have been commercially available for many years. PMTs with the same type of photocathode have been commercially available and no major lifetime issues have been reported. We are hopeful that the lifetime of these HPMTs will be comparable to that of conventional PMTs.

3. HPMT photocathode responsivity measurements

The HPMT photocathode QE was determined by measuring the photocurrent as a function of the incident light at room temperature. The light source consisted of an incandescent light bulb followed by an interference filter of about 10 nm bandwidth and centered at the desired wavelength. The light was then coupled into an optical fiber, through a programmable attenuator, and focused to a 20 μm spot on the HPMT. A beam splitter and an optical power meter were used to monitor the amount of light falling onto the detector in real time. The photocathode was biased at 1000 V and the TE bias was 2.0 V. There was no electron bombardment gain at this bias level. All other terminals including the avalanche diode were shorted together and connected to the high-voltage ground through an electrometer (Keithley 617).

Figure 3 shows the measured photocurrent as a function of the incident light. The dark current was about 5 pA after warming up. The photocathode quantum efficiency is given by $QE = \Delta I_{\text{anode}}/(qP/hf)$, where ΔI_{anode} is the total anode current minus the dark current, q is the electron charge, P is the incident light power, and hf is the photon energy. A linear fit of this data, excluding the saturated region, shows that the photocathode QE for this device is 25% at 1064 nm wavelength.

The photocathode QE as a function of the TE photocathode bias was measured and the results are plotted in Figure 4. There is a turn-on bias voltage but the shape of the curve varies from device to device. It is often required to turn on the TE photocathode bias 1 hour before the rest of the power supplies in order to achieve the highest responsivity.

Figure 5 shows the photocathode responsivity in nA nW^{-1} as a function of the light spot position across the device active area. QE can be obtained by multiplying the responsivity by 0.855 for a 1064 nm wavelength. The amount of light on the detector was about 54 pW. The light spot size on the detector was less than 20 μm full width at half maximum (FWHM), which was verified with a CCD camera. The step size of the scan is 50 μm. The test results show that photocathode diameters are 1 mm at the base and about 0.8 mm on the top with the responsivity equal to or greater than 90% of its maximum value.

4. HPMT photon-counting performance measurement

4.1. Measurement setup

The HPMT was configured for photon-counting measurement as shown in Figure 6 during the early phase of the measurements. The HPMT was placed inside a vacuum chamber and cooled by a closed-cycle

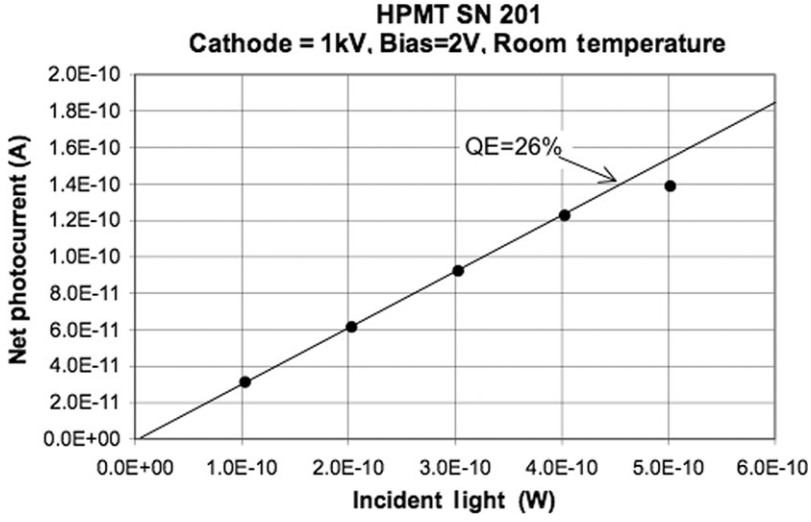

Figure 3. Net HPMT photocurrent as a function of the incident light at 1064 nm wavelength.

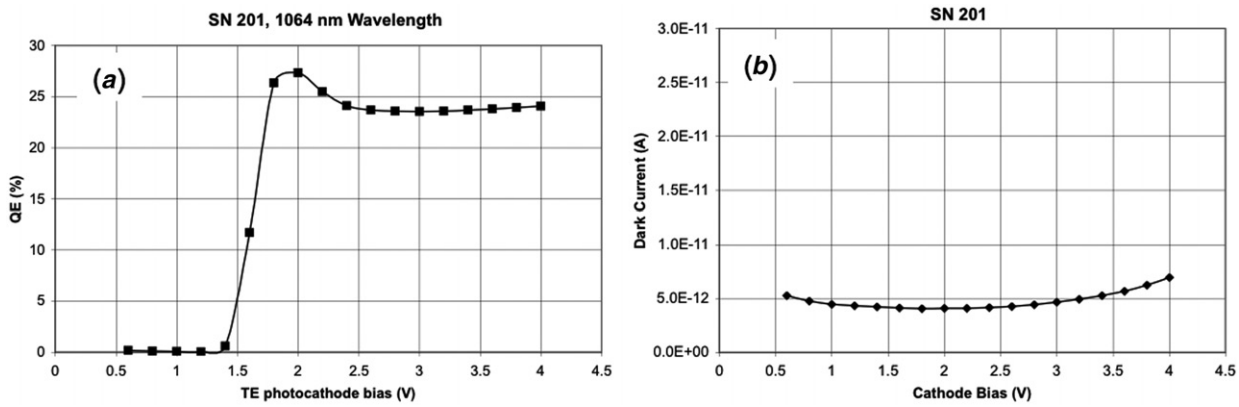

Figure 4. (*a*) QE as a function of the TE photocathode bias at 1064 nm wavelength, and (*b*) the dark current as a function of the TE photocathode bias voltage.

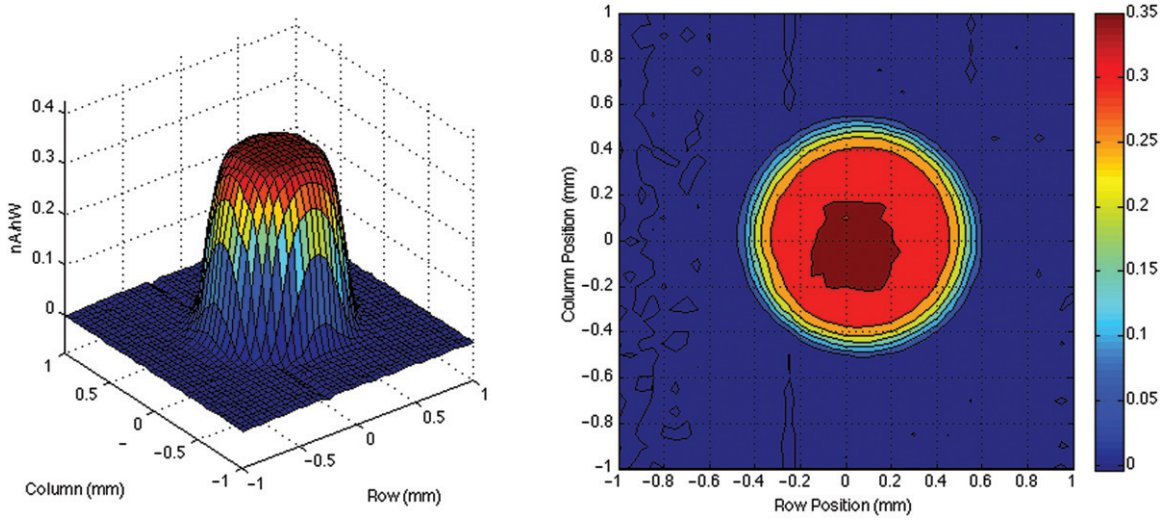

Figure 5. Photocathode responsivity in nA/nW as a function of the light spot position across the device active area. The light spot size on the detector was about 20 μm FWHM and the step size was 50 μm.

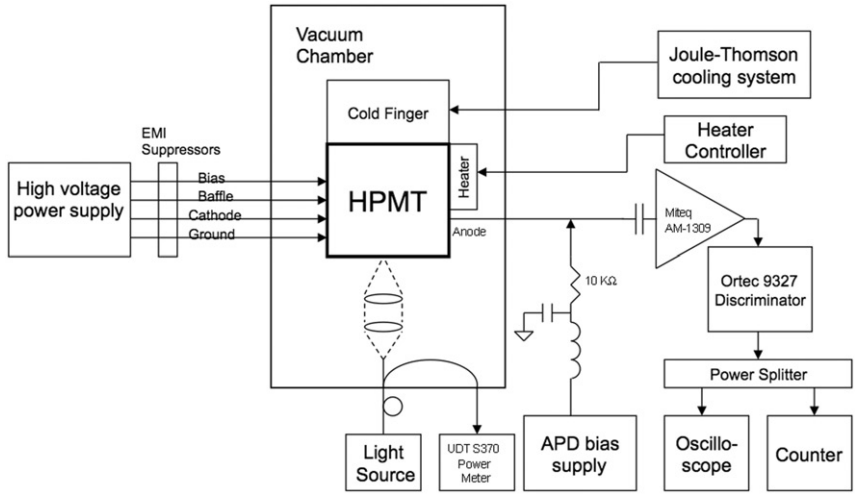

Figure 6. Test setup used in the early phase of the HPMT photon-counting testing. The Joule–Thomson cooling system and the vacuum chamber were later replaced with a TEC PMT housing.

Joule–Thomson cooling system. The device temperature was set and maintained via a set of heaters and an automatic temperature controller. The APD was reverse biased through the use of a 10 kΩ current limiting resistor. The preamplifier used was an MITEQ AM-1309 with 51 dB gain, 0.01–1000 MHz bandwidth, and 1.7 dB noise figure. The AC coupling capacitor inside the amplifier had to be replaced to accommodate the relatively high avalanche bias voltage. There was about a 1 m long coax cable between the HPMT output and the amplifier, which caused a small degradation in the signal-to-noise ratio. The noise figure of the entire system was measured to be about 3 dB. The coax cable was later replaced with a semi-rigid coax cable and the signal-to-noise ratio was significantly improved.

4.2. Avalanche diode I - V curves

The avalanche anode current as a function of the bias voltage was first measured at different temperatures and the results are plotted in Figure 7. At −20°C, the avalanche breakdown voltage is about 34 V and it varied with temperature at about 0.2 V°C^{-1}. The avalanche diode bias voltage was set to 0.9 to 0.95 times the breakdown point, or 31.5 V in this case.

4.3. Optimal discriminator threshold level

Figure 8 shows the typical pulse shape at the output of the preamplifier from a single-photon detection. The pulse amplitude varied randomly with a standard deviation equal to 15 to 20% of the mean. The pulse rise and fall time was about 0.45 ns, which implies an electrical bandwidth of 780 MHz using the empirical formula that the rise time is 0.35 times the reciprocal of the bandwidth. The preamplifier had a wider cutoff frequency (1 GHz) and should have little effect on the measurements. The pulse width was about 0.9 ns FWHM, which should be the lower limit for the HPMT dead time. In our measurements, the photon-counting dead time was actually limited by the discriminator, which had a recovery time of 10 ns. Any additional photon counts within this 10 ns dead time were not registered.

To determine the optimal threshold for the discriminator, the HPMT output count rate was measured as a function of the threshold, first in the dark and then at a constant incident light level (21.3 pW). The results for 10°C are plotted in Figure 9. Note that the threshold level in the plot was taken at the ORTEC 9327 discriminator monitor port. The actual threshold was 0.0617 times the monitored ones. Note also that the photon count pulses and the discriminator input both had negative pulse polarity. Figure 9 shows that the dark counts and the photon counts increased as the threshold level decreased. The optimal threshold is the point where the difference between the photon counts and the dark counts is the highest, or 0.4 to 0.5 V at the monitor, or 25 to 31 mV at the input. The optimal threshold at different temperatures may be determined by shifting it by the same amount as the avalanche diode breakdown voltage, or 0.2 V°C^{-1} at the input to the discriminator.

4.4. Photon-detection efficiency

The photon-counting efficiency (PDE), defined as the ratio of the number of detected photons to the number of incident photons, and the dark count rate were

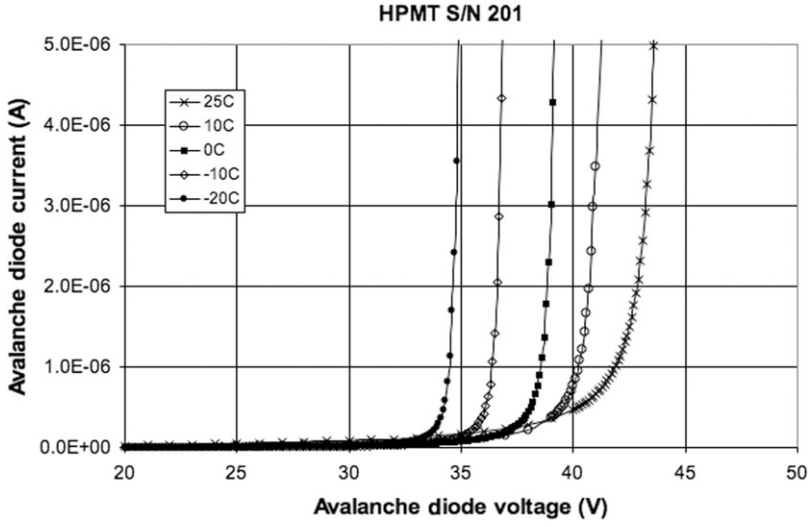

Figure 7. APD anode current as a function of the bias voltage (I–V curves) at 10, 0, −10, and −20°C.

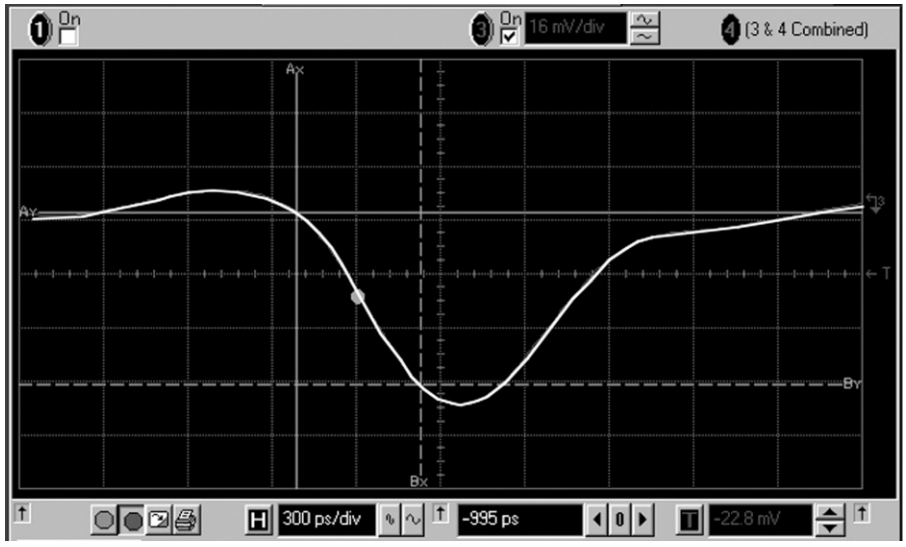

Figure 8. Typical HPMT photon count pulse shape measured at the output of the preamplifier (51 dB gain). The oscilloscope scales were set to 16 mV div^{-1} and 0.3 ns div^{-1}, respectively. The positive hump in the waveform *prior* to the pulse was probably an artifact caused by the preamplifier.

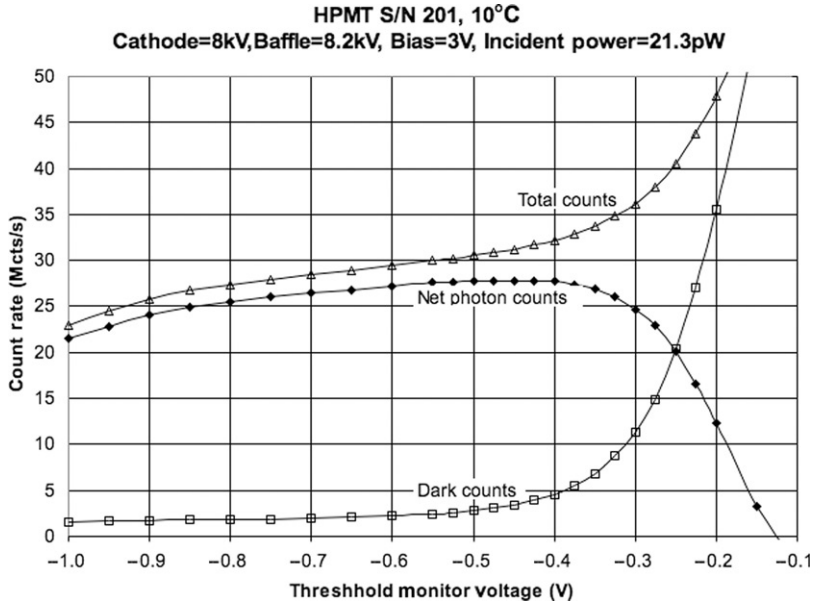

Figure 9. HPMT output count rates (green and pink) and the difference (blue) versus the discriminator threshold at dark and under 21.3 pW incident light and 10°C. The optimal threshold is shown to be −0.4 to −0.5 V. Note that the threshold level plotted was measured at the discriminator monitor port. The actual threshold level should be that multiplied by 0.0617.

measured as a function of temperature at 1064 nm wavelength and the results are plotted in Figure 10. The results show that the PDE is nearly unchanged, about 25% at 1064 nm, over the entire temperature range, and the dark count rate decreased exponentially with temperature. Furthermore, the test results in Figure 10 show that the dark count rate decreased by a factor of ten for every 24°C reduction in temperature. Although not tested by us, these HPMTs in the current package have been shown to operate at −40°C without compromising their electrical properties and mechanical integrity. Therefore, the dark count rate of the HPMTs may be further reduced by a factor of five if cooled to −40°C.

The PDE and dark count rate were also measured against other parameters, including the TE photocathode bias, APD anode bias, and photocathode voltage, and the results are shown in Figures 11–13.

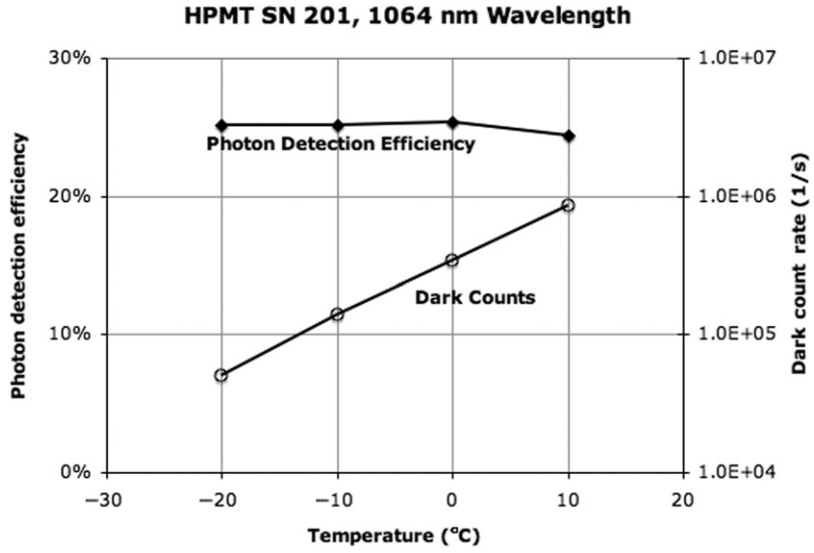

Figure 10. PDE and dark count rate of the HPMT as a function of the temperature.

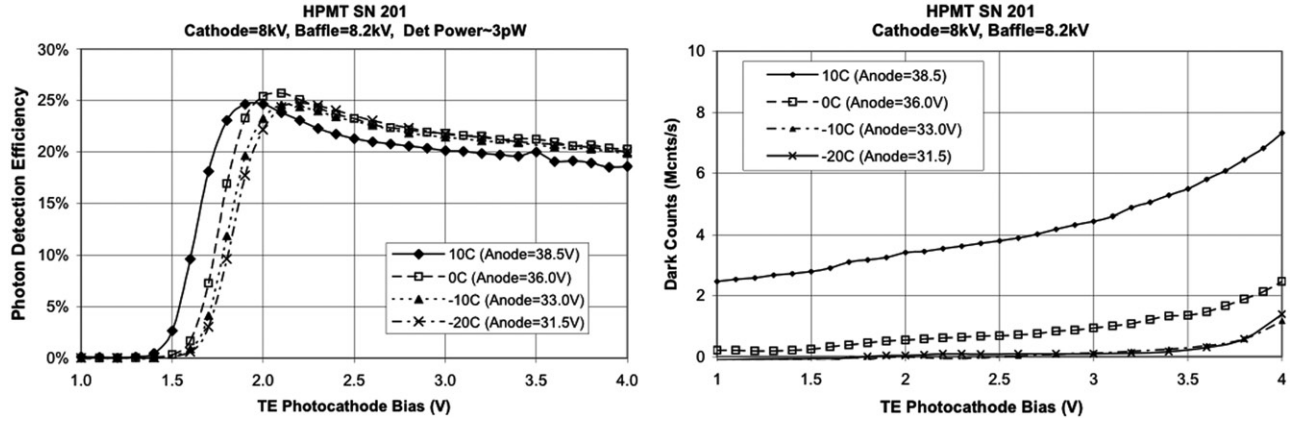

Figure 11. PDE and dark count rate of the HPMT as a function of the TE photocathode bias voltage at 1064 nm wavelength.

It was from these measurements that the optimal bias conditions were determined.

4.5. Photon-counting timing jitter measurements

The timing jitter of photon detection by the HPMT was measured using an ultra-short-pulse laser source (PicoQuant PDL 808 with a LDH-P-1060 laser head). The laser pulse width was 60 ps FWHM. The timing jitter of the test equipment was verified with a fast pulse generator and found to have a 50 ps standard deviation. The laser light was attenuated such that there was on average less than one detected photon per laser pulse. The time difference between the laser synchronization signal and the HPMT output was measured with a fast oscilloscope. The timing jitter was found to be sensitive to the TE photocathode bias voltage. Figure 14 shows a plot of the measured time jitter as a function of the photocathode bias voltage. The pulse arrival time was defined as the centroid of the pulses. As mentioned earlier, the timing jitter may be improved by reducing the thickness of the InGaAsP absorber layer.

4.6. HPMT output versus incident photons per pulse

We measured the HPMT output pulse amplitude as a function of the number of incident photons per pulse using the same short pulse width laser and the results are shown in Figure 15. Since the laser pulse width was much shorter than the HPMT impulse response, all the photons could be assumed to arrive at the same time.

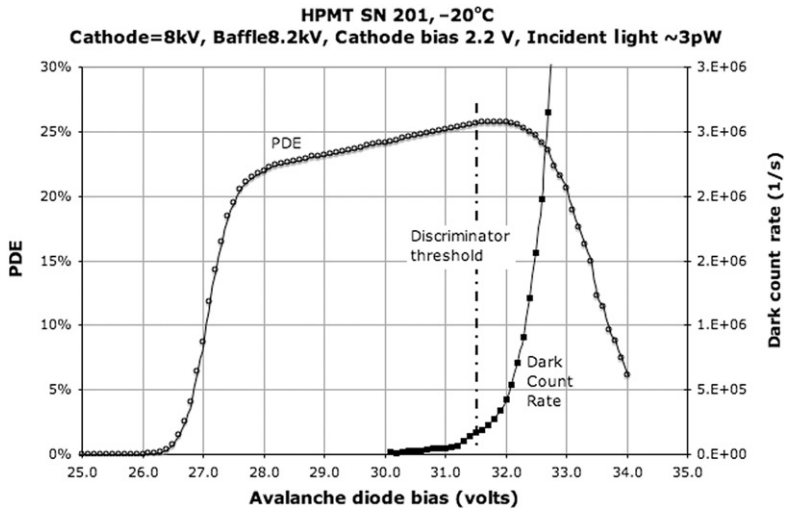

Figure 12. PDE and dark count rate versus anode bias voltage at −20°C and 1064 nm wavelength.

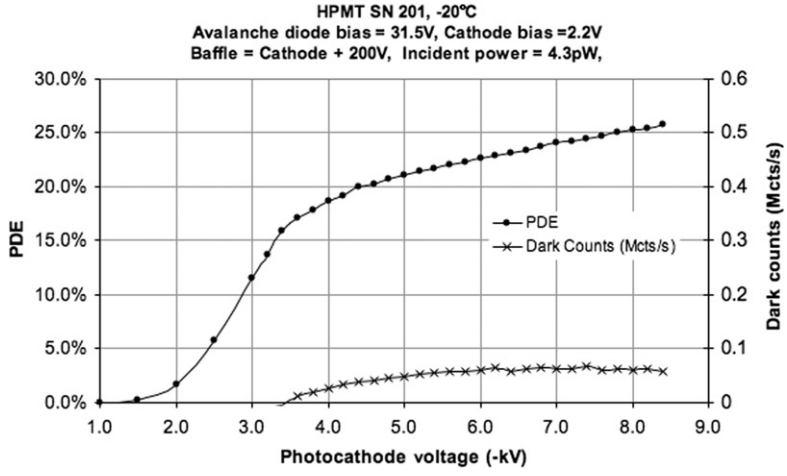

Figure 13. PDE and dark count rate as a function of the photocathode voltage at 1064 nm wavelength.

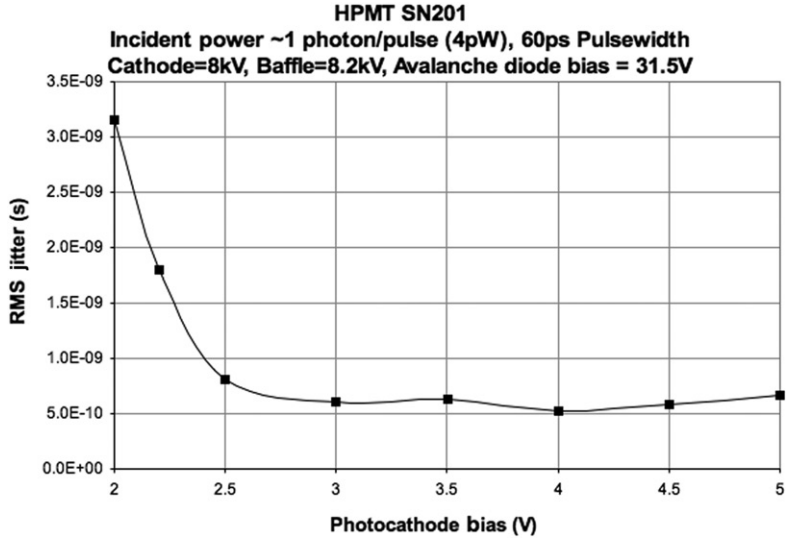

Figure 14. HPMT output timing jitter as a function of the photocathode bias voltage.

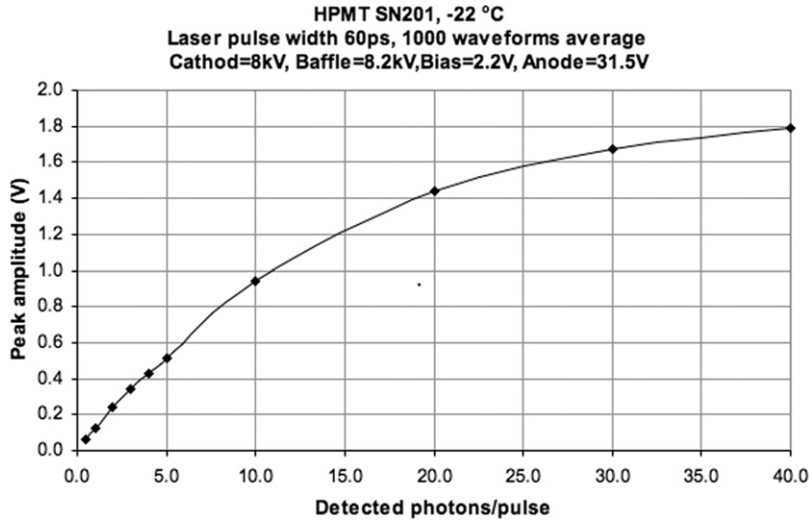

Figure 15. HPMT output pulse amplitude as a function of the number of detected photons in the incident light pulse. The roll-off at high signal level was caused by the saturation of the preamplifier.

As expected, the HPMT pulse amplitude increased almost linearly with the number of incident photons at the beginning and started to roll-off due to amplifier saturation at about 10 detected photons per pulse. The saturation was caused by the preamplifier used rather than the HPMT. The actual HPMT linear dynamic range can be as high as 1000 based on the results from other measurements at Intevac. These results indicate that one can resolve the number of photons in a pulse from the HPMT output pulse amplitude.

4.7. Afterpulsing probability

The HPMT afterpulsing was estimated from the autocorrelation function of the HPMT output counts. The HPMT output count arrival times were recorded with the use of a multichannel scaler (FAST ComTec P7887) in its single sweep mode. The light source in this case was an incandescent light bulb followed by an 1064 nm bandpass filter. The autocorrelation can then be calculated as

$$G(k) = \frac{1}{N}\sum_{i=1}^{N} n_i \cdot n_{i+k}, \tag{2}$$

where n is the photon count over the time bin at kT_{bin} and T_{bin} is the time bin width. The afterpulsing probability per time bin is given by

$$P(k) = \frac{G(kT_{bin}) - G(\infty)}{G(0) - G(\infty)}. \tag{3}$$

Figure 16 shows the measurement results with a 5 ns bin width and approximately 2.8 million counts per second. The afterpulsing at the first time bin (5 ns) shown in Figure 16 was caused by the ringing at the tail of the pulses due to impedance mismatch at the input of the multichannel scaler, not by the HPMT. The discriminator had a 10 ns dead time and could not have an output of more than one pulse within 10 ns. There was no measurable afterpulsing from 10 ns to 1 μs.

Figure 17 shows the histogram of the counts under the same test conditions and a theoretical Poisson distribution of the same mean number of counts. The close agreement between the measurement and theory further proves that the HPMT outputs were from single-photon detections and there were little nonlinear effects.

4.8. Photon-counting spectral response and output dynamic range

We also measured the PDE as a function of the wavelength of the incident light. The light source was an incandescent light bulb followed by a set of interference bandpass filters with about 10 nm FWHM passband. Figure 18 shows the measurement results.

Finally, the HPMT output count rate was measured as a function of the incident photon rate at 1064 nm wavelength. Figure 19 shows the net photon count rate versus the incident photon count rate at −22.5°C. The dark count rate was 50 to 60 thousand counts per second and the maximum count rate reached 100 million counts per second, which was the limit of the discriminator (10 ns dead time). The actual device dead time was limited by the impulse response

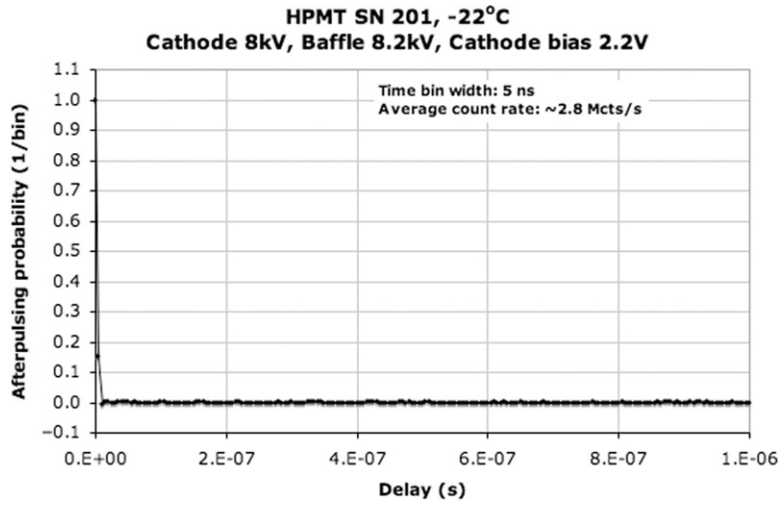

Figure 16. HPMT afterpulsing probability per 5 ns time bin.

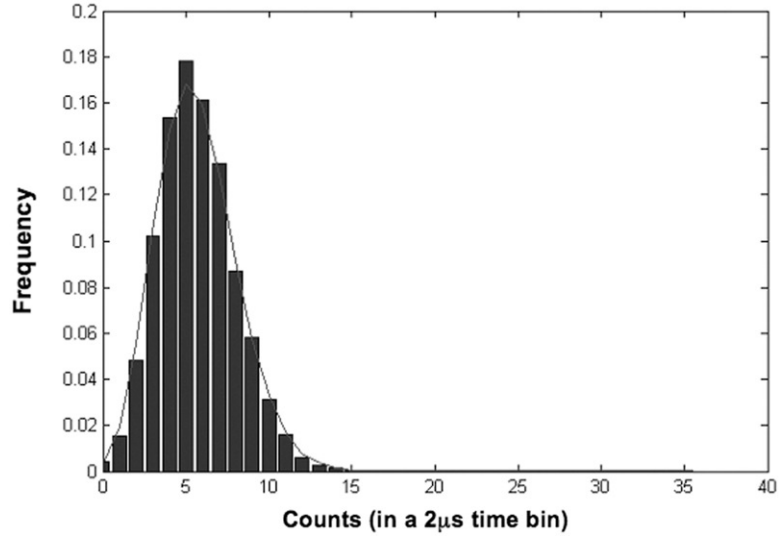

Figure 17. HPMT output count distribution along with a Poisson distribution of the same average count rate.

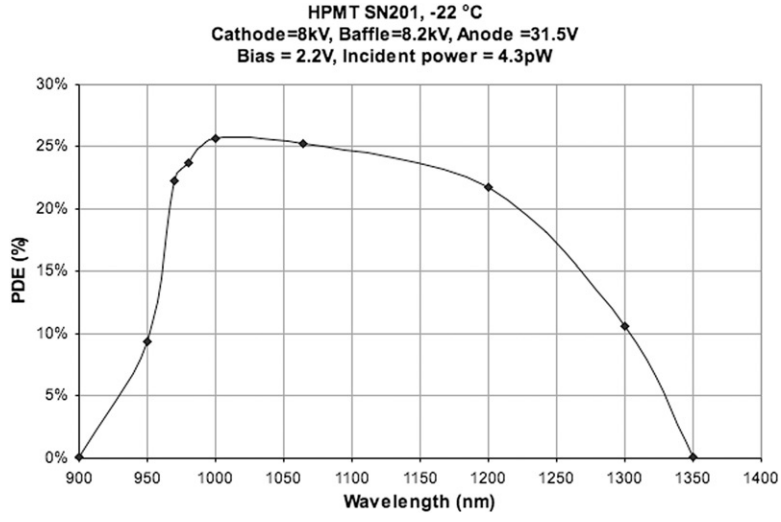

Figure 18. HPMT PDE versus wavelength.

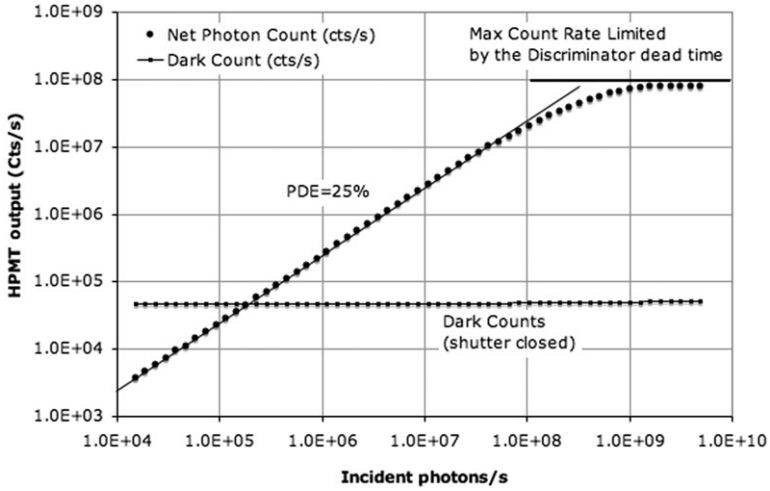

Figure 19. HPMT net photon count rate versus the incident photon rate.

width (0.8 ns FWHM). We observed consecutive photon pulses 1 to 2 ns apart on an oscilloscope while illuminating the HPMT with 6 ns laser pulses.

5. Summary

We have demonstrated that an InGaAsP TE photocathode HPMT can have a 25% PDE at a 1064 nm wavelength, 60,000 per second dark count rate, a few nanosecond dead time, 780 MHz electrical bandwidth, a wide dynamic range, 0.8 to 1 mm active area, and no afterpulsing. Such devices should have many applications where non-gated operation is required, including laser altimeters, atmospheric lidars, and free-space laser communication systems.

Acknowledgements

We thank William H. Farr of the Jet Propulsion Laboratory for sharing his experience and measurement results of similar HPMTs. We thank Dick Lavine of Intevac, Inc., for his help in obtaining the devices. This work was supported by the Instrument Incubator Programs of the NASA Earth Science Technology Office and the Space Communication and Navigation Technology Program.

References

[1] Thermalelectric Cooled NIR-PMT Module H10330-25, −45, −75; Hamamatsu Photonics K.K., Electron Tube Division, 2006 (datasheet).

[2] Biswas, A.; Farr, W. *The Interplanetary Net work Progress (IPN) Progress Report;* Jet Propulsion Laboratory, California Institute of Technology: Pasadena, CA, 2004; pp 42–152, Febuary 2004.

[3] Campbell, J.C.; Wang, S.; Zheng, X.; Li, X.; Li, N.; Ma, F.; Sun, X.; Collins, C.J.; Beck, A.L.; Yang, B., et al. *Proceedings of SPIE* **2003,** *5246,* 375–388 (Keynote Address).

[4] Cova, S.; Ghioni, M.; Lotito, A.; Rech, I.; Zappa, F. *J. Mod. Optics* **2004,** *51,* 1267–1288.

[5] Pellegrini, S.; Warburton, R.E.; Tan, L.J.J.; Jo Shien, Ng; Krysa, A.B.; Groom, K.; David, J.P.R.; Cova, S.; Robertson, M.J.; Buller, G.S. *IEEE J. Quantum Electron.* **2006,** *42,* 397–403.

[6] Donnelly, J.P.; Duerr, E.K.; McIntosh, K.A.; Dauler, E.A.; Oakley, D.C.; Groves, S.H.; Vineis, C.J.; Mahoney, L.J.; Molvar, K.M.; Hopman, P.I., et al. *IEEE J. Quantum Electron.* **2006,** *42,* 397–403.

[7] La Rue, R.A.; Sykora, D.F.; Jurkovic, M.J.; Aebi, V.W. *Military Sensing Symposia;* (MSS) Specialty Group on Active EO Systems: Monterey, CA, 2006, September 26–28, Session F, Paper AF14.

[8] Costello, K.; Aebi, V.; Davis, G.; La Rue, R.; Weiss, R. *Proceedings of SPIE* **1995,** *2550,* 177–188.

[9] La Rue, R.A.; Davis, G.A.; Pudvay, D.; Costello, K.A.; Aebi, V.W. *IEEE Electron Device Lett.* **1999,** *20,* 126–128.

[10] La Rue, R.A.; Costello, K.A.; Davis, G.A.; Edgecumbe, J.P.; Aebi, V.W. *IEEE Trans. Electron Devices* **1997,** *44,* 672–678.

[11] Kalibjian, R. *IEEE Trans. Nuclear Sci.* **1965,** *NS-12,* 367–369.

[12] DeSalvo, R.; Hao, W.; You, K.; Wang, Y.; Xu, C. *Nuclear Instrum. Methods Phys. Res.* **1992,** *A315,* 375–384.

[13] Sun, X.; Davidson, F.M. *J. Lightwave Technol.* **1992,** *10,* 1023–1032.

[14] Cushman, P.; Rusack, R. *Nuclear Instrum. Methods Phys. Res.* **1993,** *A333,* 381–389.

[15] Suyama, M.; Lares, M. *Laser Focus World* **2008,** *3,* 80–84.

[16] Farr, W.H. *2005 Digest of the LEOS Summer Topical Meeting;* San Diego, CA, 2005, July 25–27, pp 17–18.